6-2004

Multi-scale continuum mechanics: from global bifurcations to noise induced high-dimensional chaos

Ira B. Schwartz
Naval Research Laboratory

David S. Morgan
Naval Research Laboratory

Lora Billings
Montclair State University, billingsl@montclair.edu

Ying-Cheng Lai
Arizona State University

Multi-scale continuum mechanics: From global bifurcations to noise induced high-dimensional chaos

Ira B. Schwartz[a] and David S. Morgan
Naval Research Laboratory, Plasma Physics Division, Nonlinear Dynamics System Section, Code 6792, Washington, DC 20375

Lora Billings
Department of Mathematical Sciences, Montclair State University, Upper Montclair, New Jersey 07043

Ying-Cheng Lai
Department of Mathematics and Statistics, Department of Electrical Engineering, Arizona State University, Tempe, Arizona 85287

(Received 30 September 2003; accepted 13 January 2004; published online 21 May 2004)

Many mechanical systems consist of continuum mechanical structures, having either linear or nonlinear elasticity or geometry, coupled to nonlinear oscillators. In this paper, we consider the class of linear continua coupled to mechanical pendula. In such mechanical systems, there often exist several natural time scales determined by the physics of the problem. Using a time scale splitting, we analyze a prototypical structural–mechanical system consisting of a planar nonlinear pendulum coupled to a flexible rod made of linear viscoelastic material. In this system both low-dimensional and high-dimensional chaos is observed. The low-dimensional chaos appears in the limit of small coupling between the continua and oscillator, where the natural frequency of the primary mode of the rod is much greater than the natural frequency of the pendulum. In this case, the motion resides on a slow manifold. As the coupling is increased, global motion moves off of the slow manifold and high-dimensional chaos is observed. We present a numerical bifurcation analysis of the resulting system illustrating the mechanism for the onset of high-dimensional chaos. Constrained invariant sets are computed to reveal a process from low-dimensional to high-dimensional transitions. Applications will be to both deterministic and stochastic bifurcations. Practical implications of the bifurcation from low-dimensional to high-dimensional chaos for detection of damage as well as global effects of noise will also be discussed. © *2004 American Institute of Physics.*
[DOI: 10.1063/1.1651691]

Transition to chaos has been a fundamental problem in nonlinear dynamics. The well known routes to chaos, which include the period-doubling bifurcation route, the intermittency route, the quasiperiodic route, and the crisis route, are for transition to low-dimensional chaotic attractors with one positive Lyapunov exponent. Transitions to high-dimensional chaotic attractors with multiple positive Lyapunov exponents have begun to be addressed. Here we present a class of physical systems consisting of linear continuum mechanical structures coupled to nonlinear oscillators. These systems arise naturally in many important engineering and defense applications. Mathematically, such a system is typically described by a set of coupled partial and ordinary differential equations, which is generally not amenable to analysis. However, if the system exhibits intrinsically distinct time scales, approximations can be made which mathematically reduce the coupled system to a set of ordinary differential equations. Dynamically, this is equivalent to decomposing the motions into those having slow and fast time scales, allowing for numerical and physical analyses. If the coupling between the continuum component and the nonlinear oscillator is small, the dynamics can be regarded as being confined to a slow, approximately invariant manifold exhibiting low-dimensional chaos. Motions away from the slow manifold are typically fast in time, are high-dimensionally chaotic, and they become important when the coupling is large or when there is noise present. The system thus represents a paradigm for investigating fundamental phenomena in nonlinear and stochastic dynamics such as the transition to high-dimensional chaos and noise-induced high-dimensional chaotic attractors. Here we shall demonstrate that this is so.

I. INTRODUCTION

In many mechanical structures of significance, such as ships, aircraft, and space vehicles, there arise problems in multi-scale dynamics due to various physical factors.[2–5] First and foremost is that many of the structures we come to depend upon are composed of many sub-structures covering a wide range of sizes,[6] as in aircraft carriers or the space station. Second, several orders of magnitude in flexibility may be present, such as a tether attached to a satellite,[7] or different beam lengths in a large truss.[8] Such differences in spatial

[a]Electronic mail: schwartz@nlschaos.nrl.navy.mil

scales have recently led to a number of new multi-scale numerical modeling techniques, such as those applied to the finite element method.[1]

As a result of such a wide range of sizes and stiffness arising from coupled structures of differing elasticity, one expects that there should exist a range of corresponding dynamical responses in frequency. Therefore, incorporating the relevant physics together in a complex model will generate multi-scale dynamics. That is, there is a set of dynamics which may be complicated (such as high-dimensional chaos), but has definitive multi-scale structure. An excellent example of such a model is the class of driven coupled continuum mechanical structures which may be used to explore nonlinear vibrations in mechanics.

In analyzing the dynamics of coupled continuum mechanical models, one must consider them as spatio-temporal systems which may support a range of dynamical time scales. Excellent examples of multi-scale behavior have been studied in the flexible spherical pendulum,[9] the dynamics of a flexible beam-oscillator system,[10] and a flexible rod–pendulum system.[11] These examples demonstrate the idea that in addition to a temporal splitting between fast and slow time scales, there also corresponds a geometric splitting. Multi-scale behavior in mechanics is convenient since the model in many instances may be decomposed into a global singular perturbation problem.[12] Based on a well-developed theory, one may construct rescaled systems for which the dynamics, under suitable hypotheses, may reside on an invariant manifold.[13] Physically, this might occur if one structure is almost perfectly rigid (fast time scale) and attached to a flexible structure (slow time scale). An excellent example is the class of ''fast–slow'' continuum systems which consists of ''soft'' structures coupled to ''stiff'' structures.

This class of ''soft–stiff'' engineering structures can have very complicated dynamics. Since the stiff part of the problem may be considered an approximation to a perfectly rigid body, it is reasonable to assume that part of the complexity originates within the soft, flexible structure. The geometric splitting yields invariant manifolds which may include chaos within the soft structure.[14] On the other hand, for critical parameter choices, the dynamics may leave the manifold, and sample the rest of the phase space, generating a dimension changing bifurcation which includes both fast and slow time scales.[14]

Since multi-scale engineering structures may have a dimension changing bifurcation, techniques for statistically quantifying the dynamics in space are needed. One such powerful method is that of the method of snapshots, based on the proper orthogonal decomposition (POD), or Karhunen–Loeve (KL) techniques.[15,16] First introduced to handle fluid dynamics, these methods have been successful in quantifying the dynamics in fluid–structure interactions,[17] spatio-temporal feedback control,[18] nonstationary flow transition problems,[19] and aerodynamics foils.[20] They have been used to quantify a dimension change bifurcation explicitly in a soft–stiff system operating near a resonant condition. In quantifying the dynamics of a spatio-temporal system, the KL technique is a powerful tool to describe the modal structure, not only analytically but computationally as well. In contrast, if one wishes to compute dynamical dimension, such as Lyapunov dimension,[21] the linear variational equations need to be solved along the trajectory, which is prohibitively expensive even for a modest system of ordinary differential equations (ODEs).

Although the KL methods are useful for quantifying a dimension change in dynamics, they do not necessarily explain the underlying cause of the bifurcation. In particular, when we think of a dimension bifurcation, we think of a change in dimension, abrupt or continuous, as a parameter is changed. Normally, the parameter is changed deterministically, resulting in a change in bifurcation structure. This may be explained as sufficiently sampling parts of an attractor off of an invariant manifold. Such bursting is typically observed to be chaotic, which arises from an underlying deterministic chaotic saddle.[22] However, another cause of dimension changing chaos may be stochastic. That is, if sufficient noise is added to a low-dimensional attractor, it may generate a high-dimensional noise induced attractor with a new positive Lyapunov exponent. Noise induced chaos, when produced along with a dimension changing bifurcation, could cause multi-scale behavior in continuum mechanics. Associated with noise induced chaos is the idea of unstable dimension variability (UDV).

Unstable dimension variability is the changing of the number of local unstable directions along a typical trajectory. Mathematically, it can be described in terms of how a system violates the properties of hyperbolicity. This nonhyperbolicity has been shown to be fundamental to chaotic dynamics, particularly for the problem of shadowing of numerical trajectories in higher dimensions.[23–30] In Ref. 31, we reported on noise induced chaos in a preliminary mechanics example. There, noise was used to excite a positive Lyapunov exponent.

In this paper, we report on the status of dimension changing bifurcations in both deterministic and stochastic mechanical systems. As such, some of the material is necessarily review. The paper is laid out as follows: In Sec. II, the full model of a rod–pendulum system is derived as a nonlinear coupled PDE–ODE system. A Galerkin projection is done to put the model in terms of an infinite system of ODE's, and then a finite dimensional model is extracted to study the dynamics. In Sec. III, the bifurcation structure is presented for the deterministic systems derived in Sec. II. Evidence of UDV is presented in the continuation diagrams. Section III C explores dimension change bifurcations based on KL methods, as well as Lyapunov spectra. Section IV explores the effects of noise on the dynamics.

II. DYNAMICAL CONTINUUM MECHANICS

In general, the problems we consider here model linear continua coupled to nonlinear oscillators. That is, the problem class is that of linear PDE's which are coupled to one or more nonlinear oscillators represented by ODE's. Such linear–nonlinear coupled systems are ubiquitous in many applications, and are observed to exhibit nonlinear vibrations in experiments.[10] In this section, we restrict ourselves to models of linear elastica in one spatial dimension. Such examples

include cantilevered beams and extensible rods. In general, if we let $W(\xi,t)$ denote a measure of displacement as a function of space (ξ) and time (t), and let $\varkappa_\mu(\xi,t)$ be a forcing function, then the general equations of motion may be represented as

$$L_\mu W(\xi,t)=\varkappa_\mu(\xi,t),$$
$$\frac{d^2\theta}{dt^2}+[1+G(W_{,tt})]\sin\theta+\eta\frac{d\theta}{dt}=0, \tag{1}$$

plus the appropriate boundary conditions. In Eq. (1), θ denotes the angular position of an attached pendulum at a free end of the elastica. The term $G(W_{,tt})$ is the additional acceleration imposed on the pendulum from the structure. Since there is an external driving body force on the structure, the function $G(W_{,tt})$ will also contain a time varying source, which will in general depend on another oscillator, such as a mechanical shaker or periodic electric potential.

The differential operator, L_μ, is assumed to be linear, and depends on a parameter which is a measure of spectral splitting of the relevant time scales. For a cantilevered beam, it has the form

$$L_\mu W=\mu^2\kappa_1^2 W_{,tttt}+W_{,\xi\xi\xi\xi}+2\zeta_b\mu W_{,t\xi\xi\xi}, \tag{2}$$

while for an extensible rod (detailed below)

$$L_\mu W=\mu^2 W_{,tt}-W_{,\xi\xi}+2\zeta_r\mu W_{,t\xi\xi}. \tag{3}$$

Normally, the external drive is decoupled from the rest of the structure. That is, it is assumed that the external drive is one-way coupled to the structure. In this paper, we allow the frequency dependence of the drive to depend weakly on the dynamics of the structure itself.

A. Full PDE–ODE system

In formulating the dynamics of such a mutually coupled system, we follow Refs. 13 and 22 in formulating in detail a system based on Eq. (3). We consider a specific mechanical system consisting of a vertically positioned viscoelastic linear rod of density ρ_r, with cross-section A_r and length L_r, with a pendulum of mass M_p and arm length L_p coupled at the bottom of the rod and where the rod is forced from the top harmonically with frequency Ω and magnitude α.[13] The rod obeys the Kelvin–Voigt stress–strain relation[32] and E_r and C_r denote the modulus of elasticity and the viscosity coefficient. C_p is the coefficient of viscosity (per unit length) of the pendulum and g is the gravitational constant of acceleration. The pendulum is restricted to a plane, and rotational motion is possible. The system is modeled by the following equations:

$$M_pL_p\ddot{\theta}+M_p[g-\ddot{x}_A-\ddot{u}_B]\sin(\theta)+C_pL_p\dot{\theta}=0,$$
$$A_r\rho_r\ddot{u}(x,t)-A_rE_ru''(x,t)-A_rC_r\dot{u}''(x,t)$$
$$-A_r\rho_r(g-\ddot{x}_A)=0, \tag{4}$$

where $\dot{}\equiv\partial/\partial t$, and $'\equiv\partial/\partial x$, with boundary conditions

$$u(x=0,t)=0,\quad A_rE_r\frac{\partial u}{\partial x}\bigg|_{x=L_r}=A_rE_r\frac{\partial u_B}{\partial x}=T_p\cos(\theta),$$

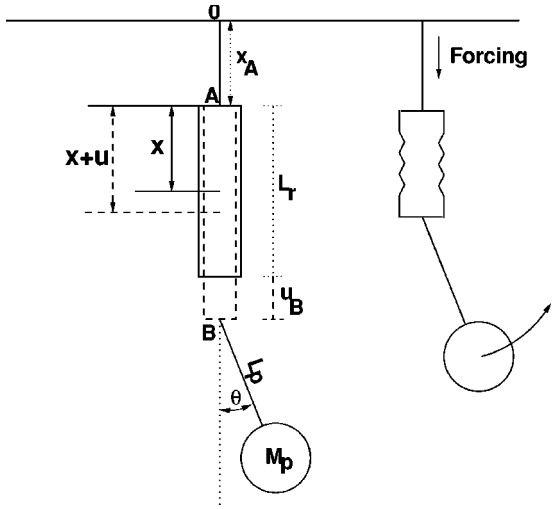

FIG. 1. Rod–pendulum configuration.

and where

$$T_p=M_pL_p\dot{\theta}^2+M_p(g-\ddot{x}_A-\ddot{u}_B)\cos(\theta),$$

denotes the tension acting along the rigid arm of the pendulum. The variable $u(x,t)$ denotes the displacement field of the uncoupled rod with respect to the undeformed configuration at equilibrium, relative to the point A, while u_B denotes the relative position of the coupling end B of the rod with respect to point A. See Fig. 1 for a schematic of the rod and pendulum system.

We further suppose that the drive at A, given by the function $x_A(t)$ in Eq. (4), is such that it comes from another oscillator. We suppose that the oscillator is weakly coupled to the pendulum through its frequency. Specifically, we model the drive oscillator by

$$\dot{\Phi}_1=\Phi_1+\Omega(1+\Sigma P(\dot{u}(x,t)))\Phi_2-\Phi_1(\Phi_1^2+\Phi_2^2)$$
$$\equiv \mathsf{F}_1(\Phi_1,\Phi_2,\Sigma,\Omega),$$
$$\dot{\Phi}_2=-\Omega(1+\Sigma P(\dot{u}(x,t)))\Phi_1+\Phi_2-\Phi_2(\Phi_1^2+\Phi_2^2)$$
$$\equiv \mathsf{F}_2(\Phi_1,\Phi_2,\Sigma,\Omega), \tag{5}$$

where P is a projection onto a Fourier mode (see below), and $|\Sigma|\ll 1$ is the coupling term that modulates the frequency. Notice that when $\Sigma=0$, the solution of Eq. (5) consists of sines and cosines of frequency ω given the appropriate initial conditions. In terms of the solutions to Eq. (5), note that $x_A(t)=\Phi_2(t,\Sigma)$.

Equations (4) and (5) are nondimensionalized by the following variable rescalings:

$$\xi=\frac{x}{L_r},\quad \tau=\omega_p t,$$
$$X_A=\frac{x_A}{L_p},\quad U=\frac{u}{L_p},\quad U_B=\frac{u_B}{L_p},$$

and parameter rescalings

$$\mu=\frac{\omega_p}{\omega_1},\quad \mu_m=\frac{\omega_1}{\omega_m}=\frac{1}{2m-1},\quad \beta=\frac{M_p}{A_r\rho_rL_r},$$

$$\zeta_p = \frac{1}{2\omega_p}\frac{C_p}{M_p}, \quad \zeta_r = \frac{1}{2\omega_1}\frac{\pi^2 C_r}{4L_r^2\rho_r},$$

where

$$\omega_p = \sqrt{\frac{g}{L_p}}, \quad \omega_m = \frac{\pi(2m-1)}{L_r}\sqrt{\frac{E_r}{\rho_r}}, \quad m = 1,2,\ldots,\infty,$$

are the natural frequency of the uncoupled pendulum and the spectrum of natural frequencies of the uncoupled flexible rod, respectively, while ζ_p and ζ_r denote their damping factors.

Using the parameter rescalings, and setting time derivatives equal to zero, the stable and unstable static equilibrium configurations of the coupled rod and pendulum system are given by $(\theta_c, \hat{U})$ and $(\theta_{S_\pm}, \hat{U})$, where

$$\theta_c = 0, \quad \theta_{S_\pm} = \pm\pi,$$

$$\hat{U} = \frac{\mu^2\pi^2}{2}[2(1+\beta)\xi - \xi^2].$$

The normalized equations are thus

$$\begin{aligned}
&\ddot{\theta} + [1 - \ddot{V}_B(\tau) - \ddot{X}_A(\tau)]\sin(\theta) + 2\zeta_p\dot{\theta} = 0,\\
&\mu^2\pi^2\ddot{V}(\xi,\tau) - V''(\xi,\tau) - 8\zeta_r\mu\dot{V}''(\xi,\tau) = -\mu^2\pi^2\ddot{X}_A(\tau),\\
&V(\xi=0,\tau) = 0, \quad V'(\xi=1,\tau) = -\mu^2\beta\pi^2[1 - T\cos(\theta)],
\end{aligned} \tag{6}$$

where

$$V(\xi,\tau) = U(\xi,\tau) - \hat{U}(\xi), \quad 0 \leqslant \xi \leqslant 1, \quad -\infty < \tau < +\infty,$$

and note that we redefine $\dot{} \equiv \partial/\partial\tau$ and $' = \partial/\partial\xi$ for the remainder of the paper.

B. Projection onto a finite model

In carrying out our analysis, we will consider a reduction of the ODE–PDE system in Eq. (6). This reduction is obtained by performing a modal expansion of the rod equation, where the displacement V is expanded as $V(\xi,\tau) = \Sigma_{m=1}^{\infty}\eta_m(\tau)\phi_m(\xi)$. This results in an infinite system of coupled oscillators,

$$\begin{aligned}
\ddot{\theta} &= -\left[1 + \sum_{j=1}^{\infty}(-1)^{j+1}\ddot{\eta}_j - \ddot{X}_A(\tau)\right]\sin(\theta) - 2\zeta_p\dot{\theta},\\
L_m(\theta)\ddot{\eta}_j &= -\frac{\eta_m}{4\eta^2\eta_m^2} + 2\zeta_r\frac{\dot{\eta}_m}{\mu\mu_m^2}\\
&\quad -(-1)^{m+1}2\beta[\dot{\theta}^2\cos(\theta) - \sin^2(\theta)]\\
&\quad -\left[\frac{4\mu_m}{\pi} + (-1)^{m+1}2\beta\cos^2(\theta)\right]\ddot{X}_A(\tau),
\end{aligned} \tag{7}$$

equivalent to Eq. (4), where $L_m(\theta)$ is the infinite linear operator

$$L_m(\theta) \equiv \sum_{j=1}^{\infty}[\delta_{mj} + (-1)^{m+j}2\beta\cos^2(\theta)].$$

See Ref. 22 for the details of this transformation.

Finally, consider the finite set of ordinary differential equations obtained from Eq. (7) by truncating to the first N rod modes and applying the additional rescalings $\{\Psi_1,\Psi_2\} = \{\theta,\dot{\theta}\}$ and $\{\mu^2\mu_m^2 Z_{2m-1}, \mu\mu_m^2 Z_{2m}\} = \{\eta_m, \dot{\eta}_m\}$, obtaining

$$\begin{aligned}
\dot{\Psi}_1 &= \Psi_2,\\
\dot{\Psi}_2 &= -\left[1 - \sum_{j=1}^{N}(-1)^{j+1}f_N(\Psi,Z) - \alpha\Psi_4\right]\sin(\Psi_1)\\
&\quad + 2\zeta_p\Psi_2,\\
\dot{\Psi}_3 &= \mathsf{F}_1(\Psi_3,\Psi_4,\Sigma,\Omega),\\
\dot{\Psi}_4 &= \mathsf{F}_2(\Psi_3,\Psi_4,\Sigma,\Omega),\\
\mu\dot{Z}_{2m-1} &= Z_{2m},\\
\mu\mu_m^2\dot{Z}_{2m} &= f_N(\Psi,Z), \quad m = 1,2,\ldots,N,
\end{aligned} \tag{8}$$

where

$$\begin{aligned}
f_N(\Psi,Z) = L_{m,N}^{-1}(\Psi_1)\Bigg[&-\frac{1}{4}Z_{2m-1} + 2\zeta_r Z_{2m}\\
&-(-1)^{m+1}2\beta[\Psi_2^2\cos(\Psi_1) - \sin^2(\Psi_1)]\\
&-\left[\frac{4\mu_m}{\pi} + (-1)^{m+1}2\beta\cos^2(\Psi_1)\right]\alpha\Psi_4\Bigg],
\end{aligned}$$

Ψ_3, Ψ_4 are drive variables as defined in Eq. (5), and $L_{m,N}^{-1}(\theta)$ is the inverse of the $N\times N$ truncation of operator $L_m(\theta)$. F_1 and F_2 are given by the right-hand sides of Eq. (5). Note that Eq. (8) is an autonomous system, and the cyclic variables, Ψ_3 and Ψ_4 are introduced to account for the periodic forcing, which has period Ω when the coupling parameter $\Sigma = 0$. For this paper, unless otherwise noted, we consider the truncated system obtained by taking $N = 1$. We also considered the system in Eq. (8) with $N = 2$ and $N = 10$ and found qualitatively similar dynamics. Notice that the terms Z_{2m-1} correspond to the rod displacement amplitudes, while the even indexed terms Z_{2m} are the rod velocity mode amplitudes. The function $f_N(\Psi,Z)$ is similar to the one defined in Ref. 13 in the case where $\Sigma = 0$, and the derivation may be found there.

The primary parameter governing the coupling between the rod and pendulum is the ratio of the natural frequency of the pendulum to the frequency of the first rod mode, $\mu \equiv \omega_p/\omega_1$. In the limit $\omega_1 \to \infty$, the rod is perfectly rigid, $\mu \to 0$, and the system reduces to a forced and damped pendulum. For $0 < \mu \ll 1$ sufficiently small, global singular perturbation theory predicts that system motion is constrained to a slow manifold, and the (fast) linear rod-modes are slaved to the slow pendulum motion.[12] For nonzero α (the amplitude of the periodic forcing) the slow manifold is a nonstationary (periodically oscillating) two-dimensional surface.

For our study, we set the number of modes in the structure to be unity, and consider the following reduced system:

$$
\begin{aligned}
\dot{\Psi}_1 &= \Psi_2,\\
\dot{\Psi}_2 &= (\pi\Psi_2(-2\zeta_p - 4\beta\zeta_p\cos^2(\Psi_1) + \beta\sin(2\Psi_1)\Psi_2)\\
&\quad - \sin(\Psi_1)(4\alpha\Psi_4 + 4\alpha\beta\pi\cos^2(\Psi_1)\Psi_4\\
&\quad + \pi(1 + 2\beta + Z_1 + 2\zeta_r Z_2 + \alpha\Psi_4)))/(\pi\delta),\\
\dot{\Psi}_3 &= \Psi_3(1 - (\Psi_3^2 + \Psi_4^2)) + \Omega(1 + \sigma\Psi_2)\Psi_4,\\
\dot{\Psi}_4 &= \Psi_4(1 - (\Psi_3^2 + \Psi_4^2)) - \Omega(1 + \sigma\Psi_2)\Psi_3,\\
\dot{Z}_1 &= Z_2/\mu,\\
\dot{Z}_2 &= -(2\beta\pi - 2\beta\pi\cos(\Psi_1)\Psi_2^2 + \pi Z_1 + 2\pi\zeta_r Z_2\\
&\quad + 4\alpha\Psi_4 + 2\beta\pi\cos^2(\Psi_1)(-1 + \alpha\Psi_4))/(\mu\pi\delta),
\end{aligned}
\tag{9}
$$

where $\delta = 1 + 2\beta\cos(\Psi_1)$. In Eq. (9), Ψ_1 and Ψ_2 are the pendulum position and velocity, Ψ_3 and Ψ_4 are the drive oscillator variables, and Z_1 and Z_2 are the rod mode position and velocity. Notice that the singular perturbation parameter denotes the rod variables to have a fast time scale compared to the pendulum and drive. Also, the frequency of the drive oscillator is a function of the pendulum momentum, which is a feedback term. The system in Eq. (9) is, therefore, fully coupled, which is a generalization of the more ideal case of having a perfectly isolated drive.

III. BIFURCATION STRUCTURE OF THE DETERMINISTIC SYSTEM

We now consider the deterministic one rod mode model obtained in Sec. II. It is useful to first consider the deterministic model, without any added noise. The underlying dynamical structures of the deterministic system will determine in what way additive noise manifests itself in the dynamics. While Eq. (9) is much less complex than the original PDE, it still exhibits a wide variety of complicated behaviors. In particular, when the amplitude α of the forcing is sufficiently large, solutions of Eq. (9) are chaotic, and such solutions with both one and two positive Lyapunov exponents have been observed. In addition to the forcing amplitude α, the behavior of solutions of Eq. (9) is dramatically affected by the value of the coupling parameter μ.

Since Eq. (9) is singularly perturbed for $0 < \mu \ll 1$, we will obtain a description of the slow dynamics by closely following the geometric approach adopted in Ref. 22. The slow manifold approximation, $\{Z_1, Z_2\} = H_\mu(\Psi_1, \Psi_2, \Psi_3, \Psi_4)$ is obtained for Eq. (9) (with $\sigma = 0$), using the method of Ref. 12. The slow manifold (given by the graph of H_μ) is a submanifold in phase space on which the slow dynamics reside, and which relates the rod motion to the pendulum motion and periodic forcing. When μ is sufficiently small, the dynamics of Eq. (9) can then be approximated by the reduced system:

$$
\begin{aligned}
\dot{\Psi}_1 &= \Psi_2,\\
\dot{\Psi}_2 &= (\pi\Psi_2(-2\zeta_p - 4\beta\zeta_p\cos^2(\Psi_1) + \beta\sin(2\Psi_1)\Psi_2)\\
&\quad - \sin(\Psi_1)(4\alpha\Psi_4 + 4\alpha\beta\pi\cos^2(\Psi_1)\Psi_4\\
&\quad + \pi(1 + 2\beta + H_\mu(\cdot) + 2\zeta_r H_\mu(\cdot) + \alpha\Psi_4)))/(\pi\delta),\\
\dot{\Psi}_3 &= \Psi_3(1 - (\Psi_3^2 + \Psi_4^2)) + \Omega(1 + \sigma\Psi_2)\Psi_4,\\
\dot{\Psi}_4 &= \Psi_4(1 - (\Psi_3^2 + \Psi_4^2)) - \Omega(1 + \sigma\Psi_2)\Psi_3.
\end{aligned}
\tag{10}
$$

It is important to note that the above approximation is valid only for μ sufficiently small. In particular, it has been noticed that when μ is increased, the dynamics of the full one rod–mode system given by Eq. (9) no longer remains on the slow manifold, but exhibits a bursting characteristic. This bursting is not directly observed in the system variables themselves, but rather when observing the variable defined by $\Delta = \sqrt{(Z_1 - H_{\mu,1}(\cdot))^2 + (Z_2 - H_{\mu,2}(\cdot))^2}$, where $H_{\mu,i}(\cdot)$ denotes the ith component of H_μ. The variable Δ measures the distance of the solution of the rod components of the full problem to the slow manifold. For μ sufficiently small, only small bursts $\Delta \leqslant O(\mu)$ are observed. However, as μ is increased, the amplitude of bursts quickly increases.

Examining the variable $\Delta_1 \equiv Z_1 - H_{\mu,1}(\cdot)$ gives the difference between the actual rod displacement and the slaved rod displacement as calculated using the slow manifold approximation. As μ increases so that Δ is $O(1)$ in amplitude, Δ_1 has the appearance of a relaxation oscillation. That is, a large excursion can be observed away from the slow manifold approximation with succeeding bursts decaying in amplitude toward the slow manifold, and another large burst may occur before the solution has reached the slow manifold.

For small μ, solutions of Eq. (10) agree well with solutions of the full system modeled by Eq. (9). This ceases to be the case as μ is increased, and nontrivial fast dynamics develop. We will consider two particular choices of the coupling parameter, to illustrate the nontrivial fast dynamics which develop. In the next subsection we examine the dynamics of Eq. (9) when the coupling is relatively small: $\mu = 0.086\,875$. For this value of μ, system motion is no longer confined to the slow manifold. Instead bursting off the slow manifold is observed. We will then examine the dynamics of Eq. (9) for the relatively large value of $\mu = 0.5025$ in the following subsection. Near this value of μ there is an internal 2:1 resonance, and the observed bursting is much greater in amplitude. For the simulations presented in the remainder of this section, we set $\beta = 1$, $\zeta_r = \zeta_p = 0.01$, $\sigma = 0.0001$, and $\Omega = 1.9527$ unless otherwise stated.

A. Lyapunov exponents and attractor bifurcation structure: The singularly perturbed case

Recall that as $\mu \to 0$, there ceases to be any nontrivial rod motion whatsoever, and Eq. (9) reduces to a forced and damped pendulum. Increasing μ amounts to increasing the flexibility of the rod, and nontrivial rod motions independent of the pendulum motion are observed. For the simulations of this subsection, we set $\mu = 0.086\,875$, and vary α, while the other parameters are as stated in the introduction of this sec-

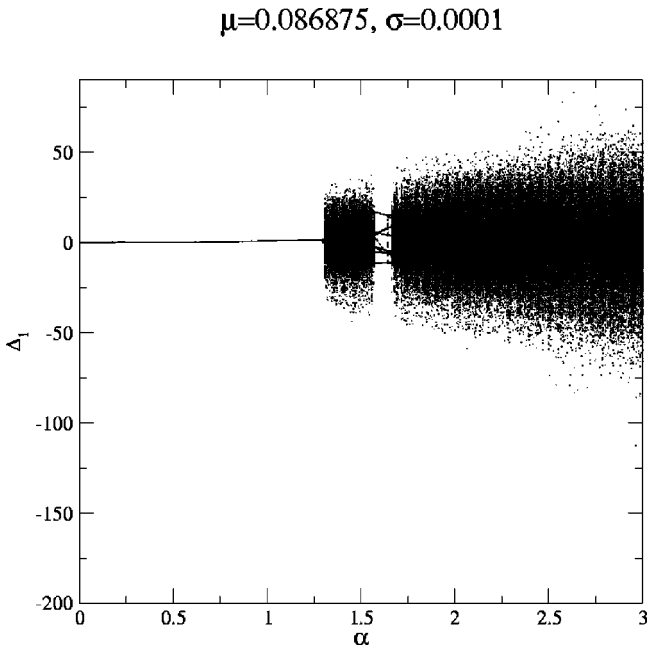

FIG. 2. The attractor bifurcation diagram for $\mu=0.086\,875$ and $\sigma=0.0001$, showing the rod displacement $\Delta_1 \equiv Z_1 - H_\mu(\Psi_1,\Psi_2,\Psi_3,\Psi_4)$ as a function of the forcing amplitude α. There is a stable periodic orbit for $\alpha \lesssim 1.30$.

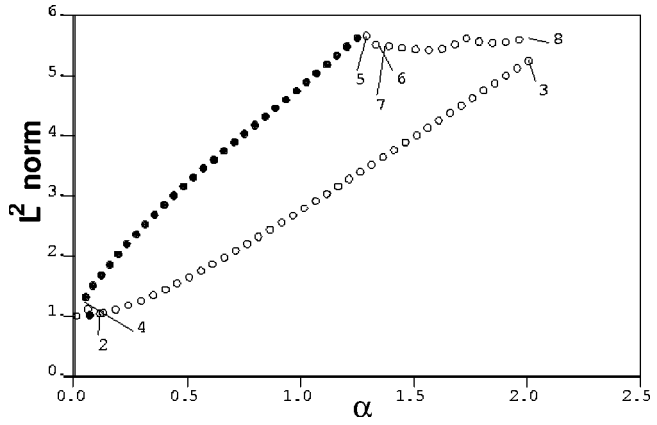

FIG. 3. The continuation diagram.. The lower branch consists of a solution in which the pendulum does not swing and only rod motion is present, while the upper branch corresponds to nontrivial periodic motion of both the pendulum and the rod. Solid dots denote a stable periodic orbit while open dots denote an unstable periodic orbit. The upper stable branch exists for $\alpha \in (0.044,1.29)$. As α increases through 1.29, stability of the periodic orbit is lost, closely corresponding with the behavior seen in Fig. 2.

tion above. We choose this value for μ because it is large enough that there is significant motion on fast time scales, but small enough that our slow manifold approximation will be reasonably accurate.

We consider first the attractor bifurcation structure of Eq. (9). In particular, we will use the bursting variable Δ_1 as a function of α. We examine the Poincaré map defined by strobing the flow whenever $\Psi_3=0$ and $\Psi_4=1$. For α sufficiently small ($\Delta_1=0$) the pendulum is stationary and only periodic motions on the fast manifold are observed. As α increases through 0.17, the pendulum transitions to periodic motion, and the resulting periodic orbit slaves the system to the slow manifold. For $\alpha \approx 1.29$, there is the sudden onset of chaos. See Fig. 2.

To further elucidate the bifurcation structure of the one mode model, we utilized the bifurcation continuation software AUTO 97,[33] using α as our continuation parameter. We started the continuation calculation using a periodic orbit we calculated numerically for $\alpha=0.01$. For this value of α, we found the stable periodic orbit to consist of a motionless pendulum and an oscillating rod mode. Physically, this corresponds to the pendulum hanging straight down, with the only motion consisting of deformations of the rod with the same period as the periodic forcing. There is a secondary branch which is born in a saddle-node bifurcation at $\alpha \approx 0.044$. The saddle branch meets the first branch of nodes at a period doubling bifurcation, while the upper branch of nodes ends at a torus bifurcation at $\alpha \approx 1.29$. This agrees closely with what is observed in the attractor bifurcation diagram. See Fig. 3.

We additionally computed the Lyapunov exponents of the one rod mode model, Eq. (9), shown in Fig. 4. The most notable feature of the Lyapunov spectrum for $\mu=0.086\,875$ is that for $\alpha \lesssim 1.75$ chaotic orbits have one positive Lyapunov exponent, while for $\alpha \gtrsim 1.75$, chaotic orbits have two positive Lyapunov exponents, and the transition from one to two positive Lyapunov exponents is smooth. This implies that as the forcing amplitude α is increased, the chaotic attractor increases in dimension.

Finally, we used the constrained invariant manifold (CIM) method exposited in Ref. 22 to compute the approximation of the stable manifold of the chaotic saddle constrained to the slow manifold. Briefly, the method works by finding those initial conditions on the slow manifold which remain within ϵ_+ of the slow manifold to time T^+ under evolution of Eq. (9). Figure 5 shows the projection of the approximated manifold onto the pendulum variables Ψ_1 and Ψ_2. This set gives an indication as to the structure of the

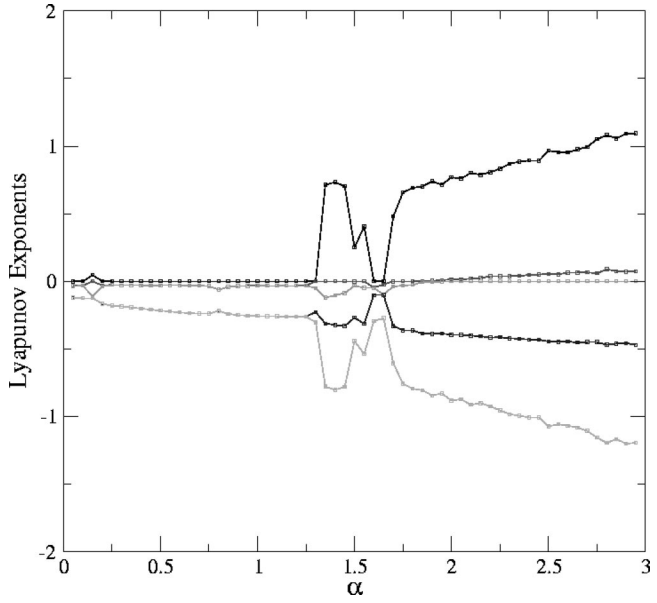

FIG. 4. The Lyapunov spectrum for $\mu=0.086\,875$. The most negative Lyapunov exponent is not shown.

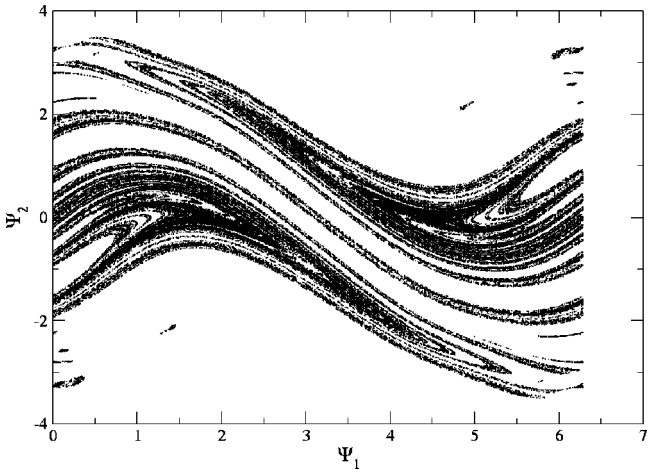

FIG. 5. The stable manifold of the chaotic saddle, constrained to the slow manifold, calculated using the CIM method and projected onto the pendulum subspace (Ψ_1,Ψ_2). The parameters used were $\mu=0.086\,875$ and $\alpha=1.2$, while β, σ, ζ_r, and ζ_p are as noted in the text.

invariants constrained to the slow manifold. The CIM method parameters used were $T^+=8.0$ and $\epsilon_+=0.1$.

B. Lyapunov exponents and attractor bifurcation structure: The near resonance case

We next increase μ to 0.5025. For this value of the coupling, there is an internal 2:1 resonance in the system.

As in the previous subsection, we consider the attractor bifurcation structure of Eq. (9), measuring the bursting variable Δ_1 as a function of α. We again use the Poincaré map given by strobing the flow whenever $\Psi_3=0$ and $\Psi_4=1$. Since μ is relatively large, we do not expect the slow manifold approximation $H_\mu(\cdot)$ to be very accurate. Indeed for α small, we observe that Δ_1 is no longer zero, but the slow manifold approximation indicates the solution lies an $O(1)$ distance from the slow manifold. However, we still expect that the observed stable periodic motions are slow. For $\alpha\approx 0.88$, there is the sudden onset of chaos, and the solutions of Eq. (9) move far from the slow manifold approximation, as shown in Fig. 6.

Using α as our continuation parameter, we started the continuation calculation using a periodic orbit we calculated numerically for $\alpha=0.01$ (see Fig. 7). For this value of α, we again find the stable periodic orbit to consist of a motionless pendulum and an oscillating rod mode. There is a secondary branch which is born in a saddle-node bifurcation at $\alpha\approx 0.044$. The saddle branch meets the first branch of nodes at a period doubling bifurcation, while the upper branch of nodes ends at a torus bifurcation at $\alpha\approx 0.27$. This agrees closely with what is observed in the attractor bifurcation diagram, as shown in Fig. 6.

Finally, we examine the Lyapunov spectrum of Eq. (9) near resonance shown in Fig. 8. The most notable feature in this case, is the sudden transition from a stable periodic orbit to hyperchaos. In fact, in numerical studies on a mesh of μ values of width 0.021 875 from $\mu=0.086\,875$ to $\mu=0.5025$, we did not observe a smooth transition from one to two positive Lyapunov exponents for any $\mu>0.086\,875$.

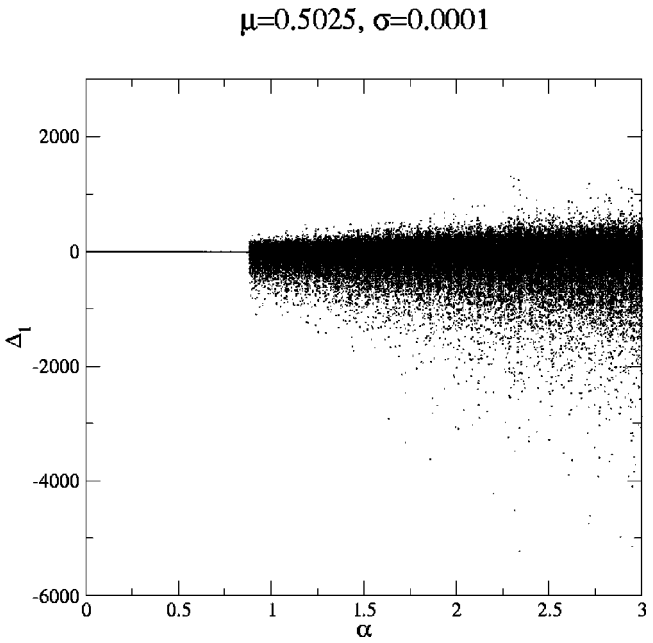

FIG. 6. The attractor bifurcation diagram for $\mu=0.5025$ and $\sigma=0.0001$, showing the rod displacement Δ_1 as a function of the forcing amplitude α. A stable periodic orbit is observed for $\alpha\lesssim 0.88$.

Rather, we observed an apparent discontinous change in the distribution of Lyapunov exponents, similar to the behavior observed in Ref. 34 where the sudden transition to hyperchaotic behavior is observed in the same model with $\sigma=0$, that is, without feedback to the drive. The transition to hyperchaos occurs near $\alpha\approx 0.88$, which agrees well with the termination of the lowest stable branch of nodes (see Fig. 7).

We again apply the CIM method to Eq. (9), this time for $\mu=0.5025$, as shown in Fig. 9. Since the system is in resonance and we are using the slow manifold approximation at the edge of its applicability, we set the threshold $\epsilon_+=150$,

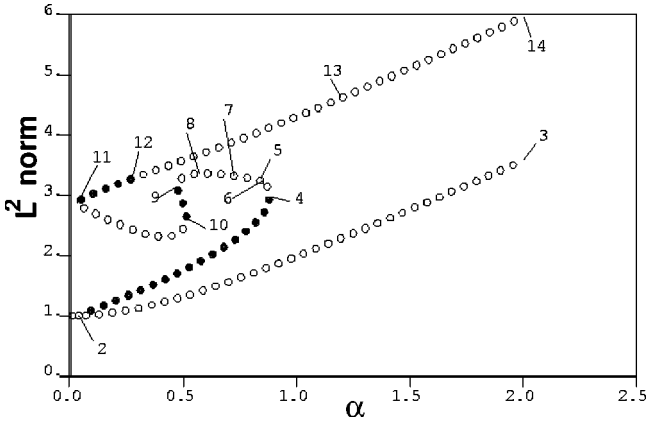

FIG. 7. The continuation diagram. The lower branch consists of a solution in which the pendulum does not swing and only rod motion is present while the upper branches corresponds to nontrivial periodic motion of both the pendulum and the rod. Solid dots denote a stable periodic orbit while open dots denote an unstable periodic orbit. Note that the lowest stable branch pictured ends in a saddle-node bifurcation (label 4) at $\alpha\approx 0.88$, corresponding to the point in the attractor bifurcation diagram (Fig. 6) where a chaotic solution is first seen.

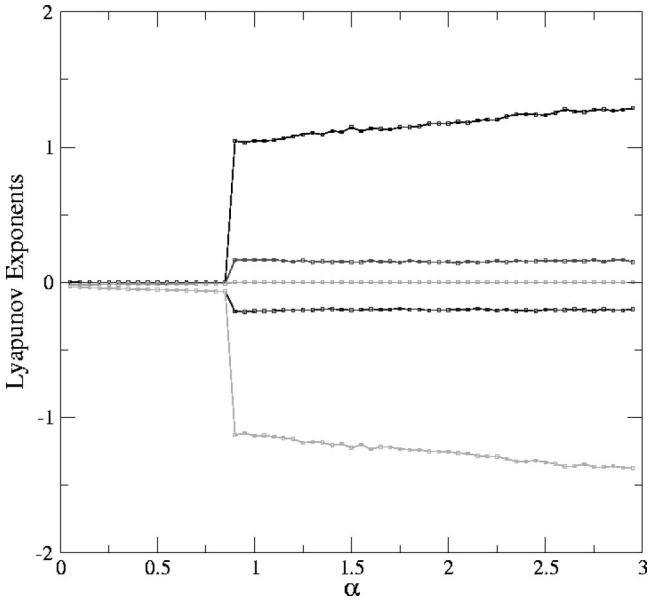

FIG. 8. The Lyapunov spectrum for $\mu=0.5025$. The most negative Lyapunov exponent is not shown.

while keeping $T^+=8$. The large value for ϵ_+ may be justified by the fact that the burst extrema observed in Δ_1 are now much larger in amplitude. There is clearly an interesting level of structure in the resulting set, though just how this set should be interpreted remains an open question.

C. Dimension changing bifurcations

In order to examine the fidelity of the one rod mode model, we examine the same model, but this time truncating the rod expansion at 16 modes. We find that while the main attractor bifurcations occur for smaller values of the forcing amplitude α, the bifurcation structure has a similar qualitative appearance to the one mode resonant case. Due to the expense of calculating the slow manifold approximation, in Fig. 10 we plot the first position rod mode against the forcing amplitude α. The behavior of the solutions is similar for what we observe in the one mode resonant case. There is a periodic orbit that abruptly transitions to a chaotic solution near $\alpha=0.32$.

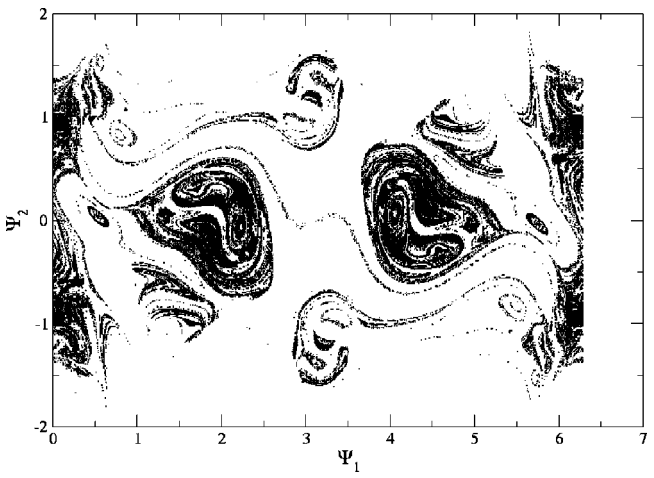

FIG. 9. The stable manifold approximation of the chaotic saddle, constrained to the slow manifold, and projected onto the pendulum subspace (Ψ_1,Ψ_2), calculated using the CIM method. The parameters used were $\mu=0.5025$ and $\alpha=0.7$, while β, σ, ζ_r, and ζ_p are as noted in the text.

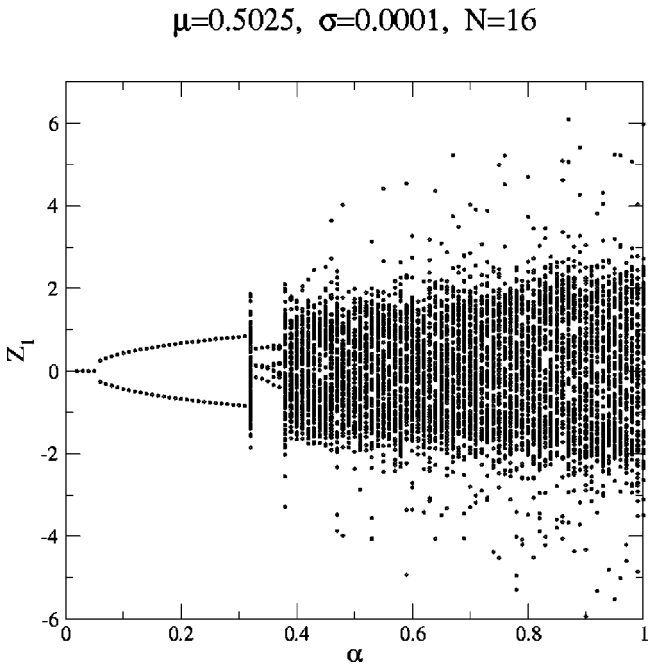

FIG. 10. The attractor bifurcation diagram for $\mu=0.5025$ and $\sigma=0.0001$ for the 16 rod mode model, showing the rod displacement as a function of the forcing amplitude α. A stable periodic orbit is observed for $\alpha\lesssim 0.32$.

We again ran AUTO on the 16 mode model as shown in Fig. 11. The saddle structure is somewhat different from that of the one mode resonant case shown in Fig. 7, but some of the essential features are still observed. In particular, the lower-most stable branch terminates in a saddle-node bifurcation near $\alpha=0.3$, close to the value for α at which we observe the first chaotic motion, as seen in Fig. 10.

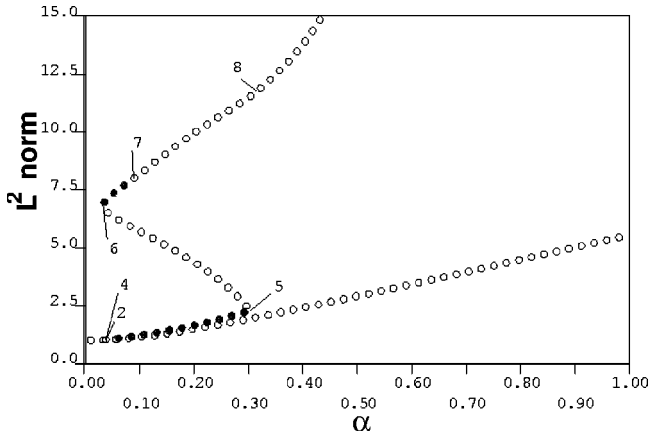

FIG. 11. The continuation diagram computed using AUTO. The lower branch consists of a solution in which the pendulum does not swing and only rod motion is present while the upper branches corresponds to nontrivial periodic motion of both the pendulum and the rod. Solid dots denote a stable periodic orbit while open dots denote an unstable periodic orbit. Note that the lowest stable branch pictured ends in a saddle-node bifurcation (label 4) at $\alpha\approx 0.3$, corresponding to the point in the attractor bifurcation diagram (Fig. 10) where a chaotic solution is first seen.

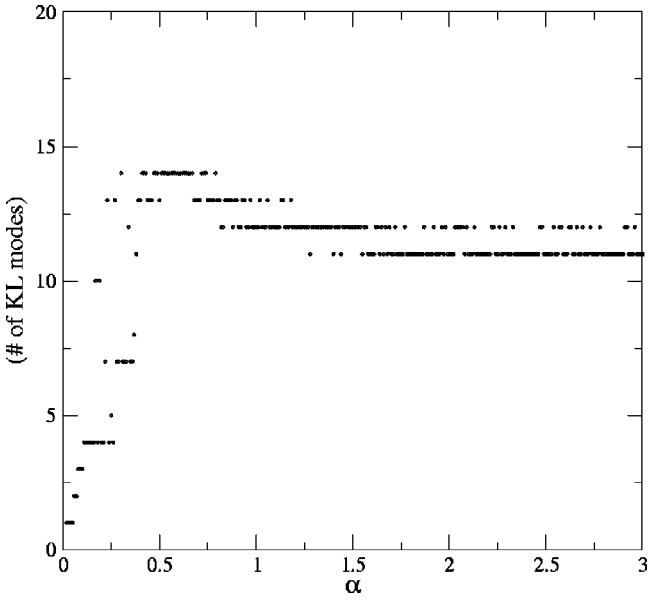

FIG. 12. The number of KL modes required to capture 99% of the system energy, as a function of forcing amplitude α.

It is expensive to calculate the Lyapunov exponents for this system, since for a system of N equations, one is required to integrate the N differential equations, plus N^2 variational equations in order to approximate the Lyapunov exponents. For the 16 mode truncation, we instead compute the KL dimension of the attractor as shown in Fig. 12. Briefly, the KL decomposition gives the optimal way to compute an orthogonal linear expansion, in an energy sense. Thus, the first mode in a KL expansion will contain the maximal energy possible for a linear mode, the second will contain the second-most energy possible, and so on. Then, a definition for KL dimension is the minimal number of KL modes required to satisfy some (large) energy threshold. Briefly, we describe how to compute the KL dimension, and the reader should see Ref. 13 for details.

We consider the system given by Eq. (8), and define the field to be the vector of continuous functions of time defined by

$$U(t)=[\Psi_1,\Psi_2,\Psi_3,\Psi_4,Z_1,Z_2,\ldots,Z_{2N-1},Z_{2N}]^T(t). \tag{11}$$

Computing the KL modes is based on a method which maximizes the variance and minimizes the covariance. For two time sampling (t_m,t_n), we define the nm entry of the correlation matrix as

$$C_{nm}=\frac{1}{NM}U^T(t_n)U(t_m). \tag{12}$$

M is the number of time snapshots, and the indices $n,m=1,2,\ldots,M$.

The ''energy'' of the system is quantified by measuring the number of active modes, which is done by gleaning information from the spectrum of the correlation matrix $\mathbf{C}$, i.e., by solving the eigenvalue problem

$$\mathbf{CA_k}=\lambda_\mathbf{k}\mathbf{A_k}. \tag{13}$$

The sum of the λ_k is the total energy of the system, and the sum is used to normalize the spectrum. That way, we can choose a threshold, say 99%, and pick those modes that are in the sum. We can then define a KL dimension of the dynamics that consists of those modes that make up 99% of the energy.

For a series of values of α, we computed the number of KL modes required to capture 99% of the system energy. We find that as α increases into the chaotic regime, the number of modes needed to capture the system energy increases dramatically. This implies that the underlying chaotic solutions are high dimensional.

IV. NOISE INDUCED CHAOS

In the previous sections, deterministic bifurcations were considered in which both low and high dimensional dynamics were observed. However, in many real engineering systems of interest, noise plays a definitive role with far reaching consequences, as seen in Refs. 35–37. In fact, it is possible to generate chaos using additive noise in mechanically driven systems, as seen in the example of driven stochastic mechanics presented in Ref. 31. In this section, we wish to take the liberty to quantify how noise induced chaos is related to a novel mathematical quantity related to the unstable dimensionality of the system. Once the dynamical systems are sufficiently high dimensional, it will be seen how noise interacts with unstable spaces to produce positive Lyapunov exponents. Since flexible continuum mechanical systems produce high dimensional dynamics, the role of noise will be seen to be play a prominent role in bifurcation theory.

A. Unstable dimension variability associated with noise-induced chaos and scaling law of Lyapunov exponents

1. Noise-induced unstable dimension variability

An interesting phenomenon associated with noise-induced chaos is that unstable dimension variability arises as soon as the attractor becomes chaotic. Unstable dimension variability means that, along a typical trajectory, the number of local unstable directions can change. This is the type of nonhyperbolicity that has been shown to be fundamental to chaotic dynamics, particularly for the problem of shadowing of numerical trajectories in high dimensions.[23–30] Mathematically, unstable dimension variability can be described in terms of the notion of hyperbolicity (or nonhyperbolicity).

Consider a chaotic set from an N-dimensional map. The set is hyperbolic if the following three conditions are met:[38] (1) At each point in the set the tangent space can be split into an expanding subspace and a contracting subspace. Distances in the expanding (contracting) subspace grow (shrink) exponentially in time; (2) the angle between the stable and the unstable subspaces is bounded away from zero; (3) the expanding subspace evolves into the expanding one along a typical trajectory and the same is true for the contracting subspace. Violation of condition (2) leads to nonhyperbolicity with tangencies, which occurs commonly in low-dimensional chaotic systems with only one unstable direction. Nonhyperbolicity with unstable dimension variability is

caused by the violation of condition (3), which occurs in systems with more than one unstable direction, i.e., high-dimensional chaotic systems. In high dimensions, commonly there are systems that violate both conditions (2) and (3).

We can argue that when noise induces a chaotic attractor, unstable dimension variability arises immediately. Consider the common situation where there are two coexisting dynamical invariant sets with distinct unstable dimensions. For instance, in the simplest case of a one-dimensional map, in a periodic window an attracting periodic orbit with zero unstable dimensions coexists with a chaotic saddle with unstable dimension one. Besides periodic windows, another situation is where there is a periodic attractor and several isolated saddle periodic orbits. The stable and unstable manifolds of these orbits are close to each other and are about to form homoclinic or heteroclinic intersections. The presence of noise can materialize the intersections, creating a chaotic set, the so-called *stochastic chaotic saddle*.[39,40]

For any periodic point on the attractor, under additive noise of amplitude D a trajectory can be found in a ball of radius D. If D is small so that the ball does not intersect the stable manifold of the chaotic saddle, the final attractor of the system will simply be a fattened version of the original periodic attractor. This is so because a random initial condition leads to a trajectory that is confined in the vicinity of the periodic attractor, although there can be transient chaos initially, in the sense that the trajectory may move toward the chaotic saddle along its stable manifold, wander near the saddle for a finite amount of time, and leave it along its unstable manifold. Assume that for $D=D_c$, the noisy ball begins to intersect the stable manifold of the chaotic saddle. For $D>D_c$, there is a nonzero probability that a trajectory in the vicinity of the original periodic attractor is kicked out of the noisy ball and moves toward the chaotic saddle along its stable manifold. Due to the nonattracting nature of the chaotic saddle, the trajectory can stay in its vicinity for only a finite amount of time before leaving along its unstable manifold and then, enter the noisy ball at the original periodic attractor again, and so on. For $D \gtrsim D_c$, the probability for the trajectory to leave the noisy ball of the original periodic attractor is small. Thus, an intermittent behavior can be expected where the trajectory spends long stretches of time near the periodic attractor, with occasional bursts out of it wandering near the chaotic saddle.

A consequence of the noise-induced intermittent behavior is that there is generally unstable dimension variability associated with a continuous trajectory. Under noise, both the chaotic saddle and the original periodic attractor belong to a single, connected dynamical invariant set. Since, in the absence of noise, periodic orbits on the chaotic saddle are all unstable and the attractor is a stable periodic orbit, noise-induced intermittency means that a trajectory moves in regions containing periodic orbits with distinct unstable dimensions. A feature that distinguishes this type of unstable dimension variability with that in the literature[23–30] is that here, the subsets with different unstable dimensions are located in distinct regions of the phase space, whereas in high-dimensional chaotic systems such as the kicked double rotor,[23,24] unstable periodic orbits in these subsets tend to mix with each other densely in the phase space.

At a fundamental level, the appearance of unstable dimension variability implies the disappearance of the neutral direction of the flow. Consider a three-dimensional flow in a periodic window, where the periodic attractor contains no unstable direction and the chaotic saddle possesses one unstable dimension. The role of noise, when it is sufficiently large ($D>D_c$), is to link these two dynamical invariant sets with distinct unstable dimensions. Now examine the local eigenplanes that contain the neutral direction of the flow associated with the periodic attractor and the chaotic saddle. In the local eigenplane at the periodic attractor, there is a stable direction and a neutral direction. Consider an eigenvector in the neutral direction. In the eigenplane of a point in the chaotic saddle, there is an unstable direction and a neutral direction. When a trajectory is driven by noise from the periodic attractor to the chaotic saddle along its stable manifold, the eigenvector can lie anywhere in the local eigenplane of the corresponding point in the chaotic saddle. After a time, the vector will be aligned in the unstable direction, due to the expanding dynamics of the chaotic saddle. Distances along the neutral direction of the original periodic attractor can no longer be preserved. This feature of a noisy chaotic attractor is fundamentally different from that of a deterministic chaotic attractor, where a neutral direction always exists. Thus we see that unstable dimension variability plays a fundamental role in shaping the topology of the noisy chaotic flow.

2. Scaling law of Lyapunov exponents

We shall argue that for noise-induced chaos, the largest Lyapunov exponent of the attractor obeys a universal algebraic scaling law:

$$\lambda_1(D) \sim (D-D_c)^{\alpha}, \quad \text{for} \quad D \gtrsim D_c, \tag{14}$$

where the scaling exponent α depends on system details. Consider an $(N+1)$-dimensional flow in a periodic window. In the absence of noise, the chaotic saddle has K_u positive, one zero, and K_s negative Lyapunov exponents ($K_u+K_s=N$) which can be ordered as follows:

$$\lambda^{S+}_{K_u} \geqslant \lambda^{S+}_{K_u-1} \geqslant \cdots \lambda^{S+}_1 > 0 = \lambda^{S0} > -\lambda^{S-}_1 \geqslant \ldots \geqslant -\lambda^{S-}_{K_s-1} \geqslant -\lambda^{S-}_{K_s}. \tag{15}$$

The periodic attractor has one zero and N negative exponents, as follows:

$$0=\lambda^{P0} > -\lambda^{P-}_1 > \cdots -\lambda^{P-}_N. \tag{16}$$

For $D<D_c$, an asymptotic trajectory is confined in the neighborhood of the periodic attractor, so the largest Lyapunov exponent of the noisy attractor is simply $\lambda_1 = \lambda^{P0}=0$. For $D \gtrsim D_c$ (after the transition to chaos), λ_1 is approximately given by

$$\lambda_1 \approx f_P(D)\lambda^{P0} + f_S(D)\lambda^{S+}_{K_u} = f_S(D)\lambda^{S+}_{K_u}, \tag{17}$$

where $f_P(D)$ and $f_S(D)$ are the probabilities that a trajectory stays near the original periodic attractor and the chaotic saddle, respectively. Because of the averaging effect of noise, we expect the dependence on noise of the largest Lyapunov

exponent $\lambda_{K_u}^{S+}$ of the original chaotic saddle to be weak. Thus the main dependence of λ_1 on noise comes from $f_S(D)$, the frequency of visit to the chaotic saddle, which is determined by the measure of its stable manifold in the noisy ball of the periodic attractor.

Consider an N-dimensional Poincaré map corresponding to the $(N+1)$-dimensional flow. For a ball of radius ϵ, the natural measure of the stable manifold contained within is proportional to

$$\epsilon^{d_s} = (\epsilon^N)^{d_s/N},$$

where ϵ^N is proportional to the volume of the ball and d_s is the information dimension of the stable manifold of the chaotic saddle. Using the Kaplan–Yorke conjecture[21] for chaotic saddles,[41] d_s is given by

$$d_s = K_s + J + \frac{H^S - (\lambda_1^{S+} + \ldots + \lambda_J^{S+})}{\lambda_{J+1}^{S+}}, \tag{18}$$

where J is an integer determined by

$$\lambda_1^{S+} + \ldots + \lambda_J^{S+} + \lambda_{J+1}^{S+} \geqslant H^S \geqslant \lambda_1^{S+} + \ldots + \lambda_J^{S+}, \tag{19}$$

and H^S is the forward entropy of the chaotic saddle:

$$H^S = \sum_{i=1}^{K_u} \lambda_i^{S+} - \frac{1}{\tau}. \tag{20}$$

Here τ is the average lifetime of the chaotic saddle on the Poincaré map. (As a practical matter, τ is in the unit of T, the average time that a typical trajectory crosses the Poincaré section.) For $D \gtrsim D_c$, the volume of the noisy ball in which the stable manifold of the chaotic saddle lies is proportional to: $(D^N - D_c^N)$. We thus have

$$\lambda_1 \sim (D^N - D_c^N)^{d_s/N} \sim (D - D_c)^{\alpha},$$

which is the scaling law (14) with the algebraic scaling exponent given by

$$\alpha = \frac{1}{N}\left[K_s + J + \frac{H^S - (\lambda_1^{S+} + \ldots + \lambda_J^{S+})}{\lambda_{J+1}^{S+}} \right]. \tag{21}$$

Numerical support for the scaling law can be found in Refs. 31 and 42.

B. Noise induced bifurcation and chaos in mechanics

We continue with two examples of how small, additive noise induces chaos and unstable dimension variability in this mechanical system. In particular, we study the transition to stochastic chaos when we add stochastic perturbations of the form

$$\frac{d\mathbf{y}}{dt} = \mathbf{F}(\mathbf{y}, p) + D\xi(t),$$

where $\mathbf{F}$ is the deterministic vector field of the mechanical system defined in Eq. (9), p represents the vector of parameters, and $D\xi(t)$ is the additive Gaussian white noise with standard deviation D. Note that $\xi(t)$ is an six-dimensional vector whose components are independent Gaussian random variables of zero mean and scaled variance. Explicitly, the noise is scaled in each component so that it does not dominate components with smaller magnitudes. We find the approximate range of each variable when it is in its steady state and then scale the standard deviation of the noise by those factors so that it effects each component equally. Noise is not added to the components representing the drive [Ψ_3 and Ψ_4 in Eq. (9)], so those variances are set to zero. We use the standard second-order Milshtein method,[43] to integrate the stochastic differential equations. We also integrate the Jacobian and calculate the Floquet multipliers to find the Lyapunov exponents based on time averaging. By fixing the parameters of Eq. (9), we examine the dynamics of the mechanical random dynamical system as the noise amplitude is increased from zero.

First, we study the system with small coupling using the parameters $\mu = 0.086\,875$ and $\alpha = 1.8$. With no noise, the dominant behavior of the system is a chaotic attractor on the slow manifold characterized by one positive Lyapunov exponent. As expected with an autonomous flow, the second largest exponent is the null Lyapunov exponent, which represents the neutral direction associated with the flow. The four remaining Lyapunov exponents are negative. Adding noise to the system excites a nearby high dimensional chaotic saddle off the slow manifold and the potential number of unstable (dynamical) dimensions is increased from one to two. Numerically, we observe that increasing the standard deviation of the noise (D) increases the third Lyapunov exponent, the largest negative exponent, in a continuous manner. When the third exponent is close to crossing zero, the null exponent increases away from zero, leaving no zero valued Lyapunov exponent within a small window. Define the beginning of this transition D_c. This fundamentally disturbs the noisy flow, resulting in two positive Lyapunov exponents and the third largest exponent approaching the zero value from the negative side. See Fig. 13(a) for a graph of this transition. We approximate the algebraic scaling of the Lyapunov exponent with a least squares fit as $a = 1.5143$, having a maximum error of 0.5786, as shown in Fig. 13(b).

Due to the small coupling parameter, the deterministic system motion is constrained to a slow manifold, which is a four-dimensional surface. The chaotic attractor resides on this surface, but random trajectories experience on–off intermittency, which is characterized by a bursting behavior off the surface. This is common for chaotic attractors having periodic orbits with unstable eigenvectors transverse to the attractor. As an orbit approaches the attractor, it sometimes lands near one of these repellors, which ejects it from the neighborhood of the attractor. Then, the trajectory visits the chaotic saddle off the slow manifold for a period of time until it begins its approach back to the attractor once again. Measuring the distance of a trajectory off the slow manifold reveals the frequency of this process, and an average bursting rate can be calculated. When noise is added to the system, the bursting rate increases with the standard deviation of the noise. This is expected since the noise facilitates the process of a trajectory landing near a repellor. If we track the Euclidean distance of the trajectory in the first two components from the slow manifold, we can set a threshold to define bursting rates. By recording the fraction of iterates in a long trajectory as a function of the standard deviation of the noise,

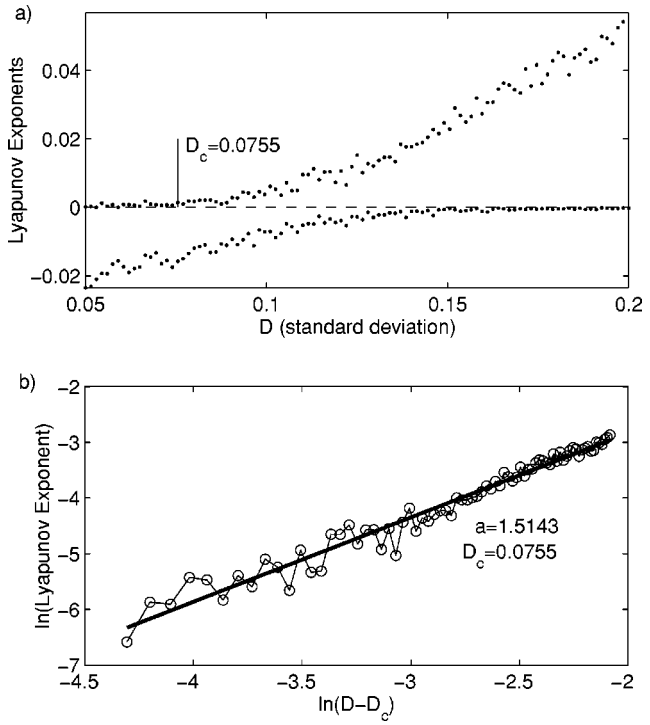

FIG. 13. For the noisy system in the small coupling case, (a) the second and third Lyapunov exponents versus D about the transition, and (b) algebraic scaling of the second largest Lyapunov exponent with $D-D_c$. The solid line in indicates the theoretical slope a.

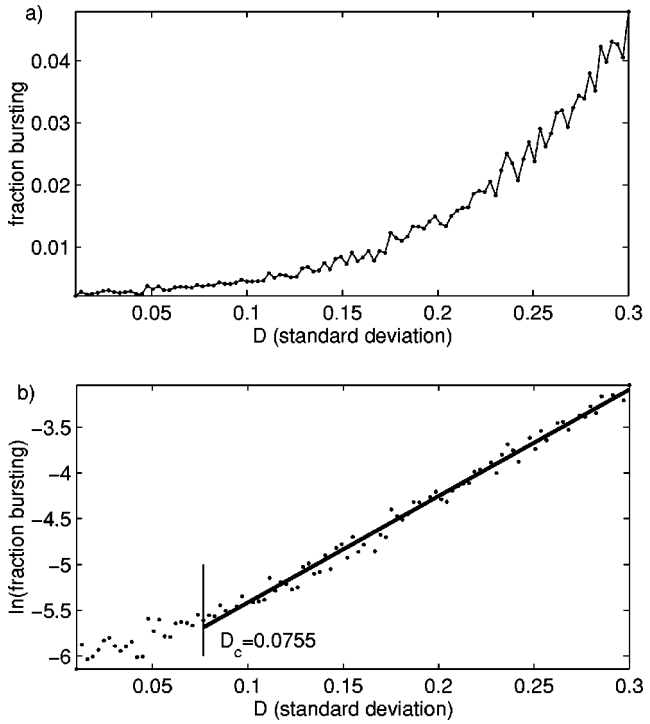

FIG. 14. For the noisy system using the parameters $\mu=0.086\,875$ and $\alpha=1.8$, (a) the bursting rate, and (b) algebraic scaling of the bursting rate. The solid line in indicates the slope.

we see a change in behavior at the same critical value D_c, where the number of positive Lyapunov exponents increase. See Fig. 14. The data follow exponential growth, and using a least squares fit, we can fit line to the natural log of the data with slope 11.6296, which has a maximum error of 0.2148, as shown in Fig. 14.

Another quantity that we can measure is the interspike interval. This is the time between bursts away from the slow manifold. Recording the interspike intervals along a random trajectory also indicates how noise increases the frequency of transients on the chaotic saddle. We calculate the interspike interval using the same threshold as the burst rate. Because the distance measurement does not have a pattern in time or amplitude, it is difficult to define the beginning and end of an individual burst. Therefore, we define the beginning of each burst as the time when the distance increases above the burst threshold. The interspike intervals are the intervals between these times. Consider the sequence of interspike intervals for a random trajectory using the parameters $\mu=0.086\,875$, $\alpha=1.8$, and $D=0.25$. The histogram of interspike interval (ISI) sequence follows a semilog scaling law. The slope of the least squares fit is -0.1275 with a maximum error of 1.9619, as shown in Fig. 15.

At larger coupling parameters, the dominant behavior of the system is a periodic attractor. Therefore, with no noise, all the Lyapunov exponents are negative except for the null exponent. The addition of noise emulates chaotic behavior, which is observed by the bifurcation in the Lyapunov exponents from zero to two local unstable directions. We use the parameters $\mu=0.5025$ and $\alpha=0.65$ as an example in Fig. 16. Notice that the two largest exponents increase in a continuous manner above zero and the third largest approaches zero from the negative side in Fig. 17(a). This is a new type of transition to noise induced chaos. The largest Lyapunov exponent follows an algebraic scaling similar to the one shown in the small coupling case. We use $D_c=0.002\,938$, which results in a linear fit with slope 1.4973 and maximum error of 0.8087. The second largest exponent also follows an algebraic scaling, but it increases from a negative value. Therefore, we must translate the Lyapunov exponent by that negative value so we can use the natural log. We use the value of the Lyapunov exponent at D_c, called L_c, and find $\ln(L-L_c)$ as we increase D from D_c. This results in a linear fit with slope 1.5090 and maximum error of 0.8198. Note the similarity in this scaling to that of the maximum Lyapunov exponent. Graphs of each of these fits are shown in Fig.

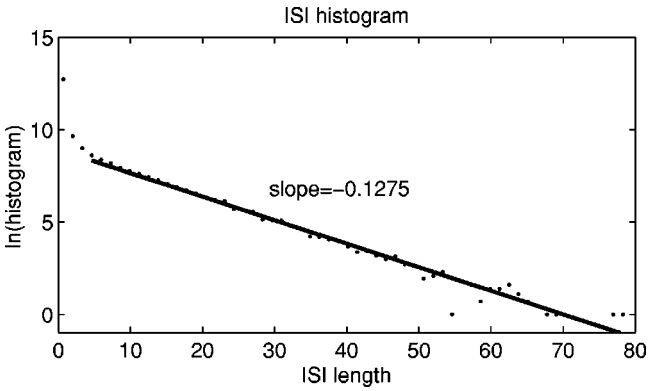

FIG. 15. The interspike interval statistics for the parameters $\mu=0.086\,875$, $\alpha=1.8$, and $D=0.25$.

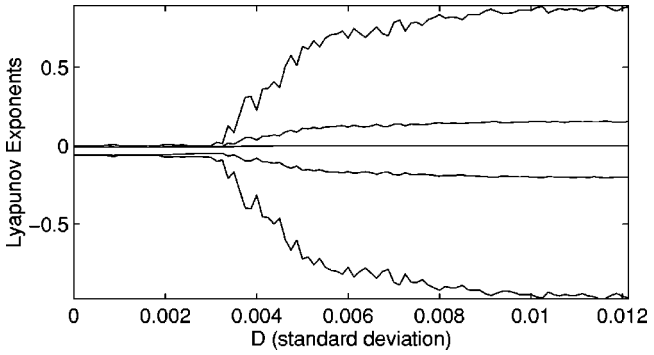

FIG. 16. The Lyapunov exponents of the noisy system. This is the large coupling case using the parameters $\mu=0.5025$ and $\alpha=0.65$.

17(b). Because this example uses a large coupling parameter, the dynamics are not dominated by the slow manifold and we cannot compute bursting statistics similar to the previous example.

V. CONCLUSIONS

We have explored a class of linear continuum mechanical systems coupled to a nonlinear oscillator from a dynamical systems point of view. In previous work, such systems were ideally driven from an outside source. In the model presented here, we considered a more general case where the frequency of the driver is slightly perturbed by the momentum change of the mechanical system to which it is connected. We have derived an ODE–PDE system describing the physics, and then showed how to construct the modal decomposition into an infinite set of ODE's. A truncated model was then derived for analysis, in which the system was described as a slow–fast time scale system, which could be analyzed using singular perturbation theory.

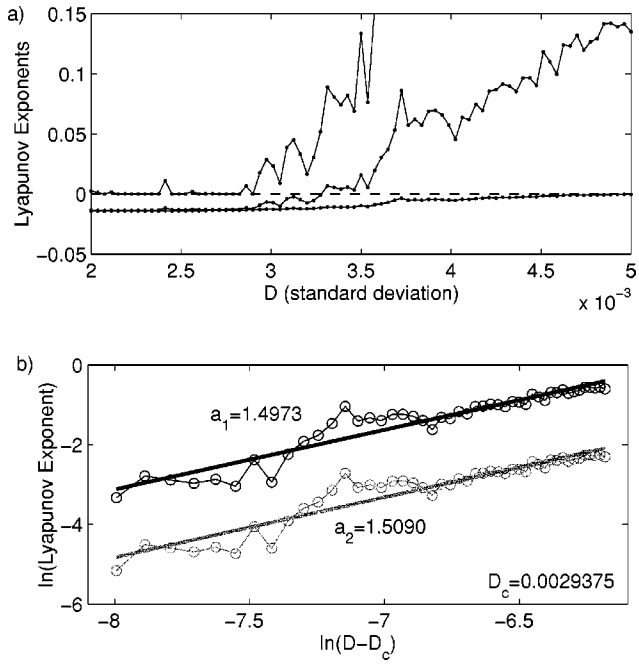

FIG. 17. These graphs use the noisy system with large coupling parameters: $\mu=0.5025$ and $\alpha=0.65$. (a) A close up of the three largest Lyapunov exponents near the transition to stochastic chaos. (b) The algebraic scaling for the two largest Lyapunov exponents. The largest exponent is shown in black and the data are plotted $\ln(L)$ vs $\ln(D-D_c)$. The second largest is in gray and the data are plotted $\ln(L-L_c)$ vs $\ln(D-D_c)$. Both linear fits have slope close to 1.5.

The deterministic system was analyzed for its bifurcation structure, which included routes to chaos, as well as torus bifurcations. However, one of the interesting bifurcations observed was that of a dimension changing bifurcation. When the singular parameter (μ) was small, one could observe chaos constrained in a neighbor of an underlying invariant manifold. However, increasing a parameter, such as amplitude a drive term in Eq. (9), would cause the dynamics to burst off the manifold into the ambient space. Accompanying sufficient bursting was the appearance of an additional Lyapunov exponent, signaling a change in dynamical dimension.

Since the invariant slow manifold is an unstable object at appropriate parameters, constraining the dynamics to the manifold reveals a chaotic saddle structure. Such a structure is important when examining both deterministic and stochastic bifurcations from low to high dimensions.

One important aspect of the noise induced bifurcation was quantifying the relationship of the change in Lyapunov exponents with respect to the standard deviation of the noise. Here we used the unstable dimension variability of the system to show explicitly in a mechanical system that the exponent obeys a universal scaling law. It is a remarkable fact that the scaling actually persists over a wide range of noise amplitudes. It is also an interesting observation that the change is continuous, even when the deterministic changes from periodic to hyper-chaotic behavior are discontinuous.

Several areas of inquiry are suggested by the current study. First, recent work has shown that sudden changes may occur as a dimension changing bifurcation when mechanical systems of sufficient complexity are operated near resonance. Since we observe such changes in simple prototypical systems, as we do here, it appears that many other systems may exhibit the same nonlinear vibrations. If so, novel controls may be designed based on the invariant manifold theory. Moreover, such control may be used to spread energy into higher heat dissipative modes, or other governing devices, making energy transfer from one part of a structure to another more efficient and directed.

On the other hand, since additive noise modifies the dynamics and its dimension continuously, it may be used a better probe for nondestructive evaluation. By comparing the pristine system to later use, one may use time series tests for nonstationarity to explore controlled frequency responses by adding noise.

Other areas of interest include nonlinear elasticity, different boundary conditions, such as clamping, and higher dimensional structures, such as trusses.

ACKNOWLEDGMENTS

I.B.S. is supported by the Office of Naval Research. D.S.M. is currently an NRC post doctoral fellow. Y.C.L. is supported by AFOSR under Grant No. F49620-03-1-0290. L.B. is supported by DARPA under Grant No. DAAD19-03-1-0134.

[1] T. J. R. Hughes, G. R. Feijoo, L. Mazzei, and J. B. Quincy, Comput. Methods Appl. Mech. Eng. **166**, 3 (1998).
[2] N. Hori and K. Seto, JSME Int. J. Ser. C **43**, 697 (2000).
[3] H. M. Mabie and C. F. Reinholtz, *Mechanics and Dynamics of Machinery* (Wiley, New York, 1986).
[4] J. D. Smith, *Gears and Their Vibration* (Marcel Dekker, New York, 1983).
[5] S. Shaw and C. Pierre, J. Sound Vib. **164**, 85 (1983).
[6] D. C. Zimmerman, Inverse Probl. **8**, 93 (2000).
[7] A. Steindl and H. Troger, Nonlinear Dyn. **31**, 257 (2003).
[8] X. H. Ma, A. F. Vakakis, and L. A. Bergman, AIAA J. **39**, 687 (2001).
[9] I. T. Georgiou and I. B. Schwartz, Nonlinear Dyn. **25**, 3 (2001).
[10] I. T. Georgiou, I. Schwartz, E. Emaci, and A. Vakakis, J. Applied Mech. Trans. ASME **66**, 448 (1999).
[11] I. T. Georgiou and I. B. Schwartz, J. Sound Vib. **220**, 383 (1999).
[12] N. Fenichel, J. Diff. Eqns. **53**, (1979).
[13] I. T. Georgiou and I. B. Schwartz, SIAM (Soc. Ind. Appl. Math.) J. Appl. Math. **59**, 1178 (1999).
[14] I. B. Schwartz and I. T. Georgiou, Phys. Lett. A **242**, 307 (1998).
[15] L. Sirovich, Physica D **37**, 126 (1989).
[16] L. Sirovich, M. Kirby, and M. Winter, Phys. Fluids A **2**, 127 (1990).
[17] A. E. Deane and C. Mavriplis, AIAA J. **32**, 1222 (1994).
[18] I. Triandaf and I. B. Schwartz, Phys. Rev. E **56**, 204 (1997).
[19] E. A. Christensen, M. Brons, and J. N. Sorensen, SIAM J. Sci. Comput. (USA) **21**, 1419 (2000).
[20] K. C. Hall, J. P. Thomas, and E. H. Dowell, AIAA J. **38**, 1853 (2000).
[21] J. L. Kaplan and J. A. Yorke, in *Lecture Notes in Mathematics*, edited by H. O. Peitgen and H. O. Walter (Springer, Berlin, 1979), Vol. 730.
[22] D. M. Morgan, E. Bollt, and I. B. Schwartz, Phys. Rev. E (to be published).
[23] S. P. Dawson, C. Grebogi, T. Sauer, and J. A. Yorke, Phys. Rev. Lett. **73**, 1927 (1994).
[24] T. Sauer, C. Grebogi, and J. A. Yorke, Phys. Rev. Lett. **79**, 59 (1997).
[25] E. J. Kostelich, I. Kan, C. Grebogi, E. Ott, and J. A. Yorke, Physica D **109**, 81 (1997).
[26] Y.-C. Lai and C. Grebogi, Phys. Rev. Lett. **82**, 4803 (1999).
[27] Y.-C. Lai, D. Lerner, K. Williams, and C. Grebogi, Phys. Rev. E **60**, 5445 (1999).
[28] E. Barreto, P. So, B. J. Gluckman, and S. J. Schiff, Phys. Rev. Lett. **84**, 1689 (2000).
[29] E. Barreto and P. So, Phys. Rev. Lett. **85**, 2490 (2000).
[30] H. Kantz, C. Grebogi, A. Prasad, Y.-C. Lai, and E. Sinde, Phys. Rev. E **65**, 026209 (2002).
[31] Y.-C. Lai, Z. Liu, L. Billings, and I. B. Schwartz, Phys. Rev. E **67**, 026210 (2003).
[32] L. Marven, *Introduction to the Mechanics of a Continuous Medium* (Prentice-Hall, Englewood Cliffs, 1969).
[33] E. J. Doedel, A. R. Champneys, T. F. Fairgrieve, and Y. A. Kuznetsov, AUTO 97: *Continuation and Bifurcation Software for Ordinary Differential Equations (with HomCont)*.
[34] I. B. Schwartz, Y. K. Wood, and I. T. Georgiou, Comput. Phys. Commun. **122**, 425 (1999).
[35] N. S. Namachchivaya and N. Ramakrishnan, J. Sound Vib. **262**, 613 (2003).
[36] N. S. Namachchivaya and H. J. Van Roessel, J. Appl. Mech. Trans. ASME **68**, 903 (2001).
[37] L. Arnold, N. S. Namachchivaya, and K. R. SchenkHoppe, Int. J. Bifurcation Chaos Appl. Sci. Eng. **6**, 1947 (1996).
[38] J. Guckenheimer and P. Holmes, *Nonlinear Oscillations, Dynamical Systems, and Bifurcations of Vector Fields* (Springer-Verlag, New York, 1983).
[39] L. Billings and I. B. Schwartz, J. Math. Biol. **44**, 31 (2002).
[40] L. Billings, E. M. Bollt, and I. B. Schwartz, Phys. Rev. Lett. **88**, 234101 (2002).
[41] B. R. Hunt, E. Ott, and J. A. Yorke, Phys. Rev. E **54**, 4819 (1996).
[42] Z. Liu, Y.-C. Lai, L. Billings, and I. B. Schwartz, Phys. Rev. Lett. **88**, 124101 (2002).
[43] S. Cyganowski, P. Kloeden, and J. Ombach, *From Elementary Probability to Stochastic Differential Equations with* MAPLE (Springer, New York, 2002).